# Ultrafast optical excitation of magnons in 2D antiferromagnets via spin torque exerted by photocurrent of excitons: Signatures in charge pumping and THz emission

Jalil Varela-Manjarres, Yafei Ren, and Branislav K. Nikolić*
*Department of Physics and Astronomy, University of Delaware, Newark, DE 19716, USA*

Recent experiments observing femtosecond laser pulse (fsLP) exciting magnons in two-dimensional (2D) antiferromagnetic (AF) semiconductors—such as CrSBr, $NiPS_3$, and $MnPS_3$, or their van der Waals heterostructures—suggest exciton-mediation of such an effect. However, its microscopic details remain obscure, as resonant coupling of magnons, living in the sub-meV energy range, to excitons, living in the $\sim 1$ eV range, can hardly be operative. Here, we develop a quantum transport theory of this effect, in which time-dependent nonequilibrium Green's functions (TDNEF) for electrons driven by fsLP are coupled self-consistently to the Landau-Lifshitz-Gilbert (LLG) equation describing classical dynamics of localized magnetic moments (LMMs) within 2D AF semiconductors. This theory explains how fsLP, of central frequency above the semiconductor gap, generates a photocurrent that subsequently exerts spin-transfer torque (STT) onto LMMs as a *nonequilibrium spintronic mechanism*. The collective motion of LMMs analyzed by windowed Fast Fourier transform (FFT) decodes frequencies of excited magnons, as well as their lifetime governed by *nonlocal* damping with the LLG equation due to, explicitly included via TDNEGF, electronic bath. The TDNEGF part of the loop is also used to include excitons via mean-field treatment, utilizing off-diagonal elements of the density matrix, of Coulomb interaction binding conduction-band electrons and valence-band holes. Finally, our theory predicts how excited magnons will *pump* time-dependent charge currents into the attached electrodes, or locally within AF semiconductor that will then emit electromagnetic radiation. The windowed FFT of these signals contains imprints of excited magnons, as well as their interaction with excitons, which could be exploited as a novel probe in future experiments.



*Introduction.*—The advent of two-dimensional (2D) magnetic materials [1, 2]—such as 2D antiferromagnetic (AF) semiconductors CrSBr [3–9], $NiPS_3$ [10], $MnPS_3$ [11] and their van der Waals heterostructures [12, 13]—has made possible recent experiments observing how femtosecond laser pulse (fsLP) excites magnons with presumed *exciton mediatation*. From a fundamental viewpoint, these experiments rekindle [14] interest in exciton-magnon coupling that was dormant [15] for many decades [16–22]. Such coupling can lead to intriguing quantum many-body effects, including magnon-magnon interactions [23, 24] dressed by excitons [5], or magnon-mediated exciton-exciton interactions [9, 25] and ultrafast exciton relaxation assisted by paramagnons [26]. As regards applications, in magnonics [27] for classical information processing, there is a considerable effort to excite coherent magnons [28, 29] by ultrafast light, whose frequencies are as high as possible and wavelengths as short as possible [11, 30]. This is because magnons with wavelength $\lesssim 100$ nm would enable miniaturization of envisaged magnonic devices down to the nanoscale [31, 32]. In contrast, oscillating magnetic fields (supplied via microstrip lines or coplanar waveguides) as standard tools are impractical for AF materials. Other schemes demonstrating excitation of AF magnons, such as by injecting current [33], lead to diffusive propagation of incoherent (at many uncontrolled frequencies) magnons. Furthermore, for quantum information processing, exciton-magnon coupling offers potential for transduction [2, 34, 35] of quantum information from qubits to microwaves that would excite magnons, and then from them, via excitons, further transduction to optical photons. In turn, photons can transfer quantum information over long distances via optical fibers [35].

The possibility of precise tuning of the central frequency of fsLP around subgap electronic states (like exciton or on-site $d$-$d$ transition [44, 45]) and thereby achieved control of excited magnons (such as dependence on light polarization [45]) emphasizes the *key role* [46] played by photoexcited electrons as mediators of magnon excitation. Thus, electrons capable of responding fast to fsLP *must be* explicitly included in any microscopic theory [47]. Their inclusion displaces often invoked [48–51], but via intuitive reasoning, direct coupling of light to local magnetization of gapped materials—this is typically a negligible effect when examined via first-principles calculations [52]. However, the first-principles derived Hamiltonians of exciton-magnon interactions are currently lacking [53]. Furthermore, extraction of magnon and exciton spectra from a single first-principles framework, such as GW methodology [54], applied to examples of 2D AF semiconductors has revealed their vastly different energy scales [54]. This means that direct (or resonant) exciton-magnon coupling is highly unlikely [55]. One could still try to devise a Hamiltonian where off-resonant coupling emerges, but this is rarely considered as it requires special conditions [55].

Lacking such inputs and microscopic nonequilibrium theory based on them, the magnon excitation aspect of recent experiments has been typically explained in phenomenological fashion [3–5, 8, 13] where "impulsive perturbation" [13] of unknown origin is inroduced into

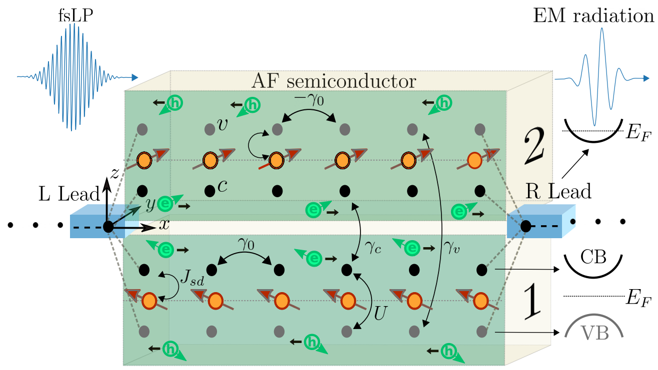


FIG. 1. Schematic view of a two-terminal setup for TDNEGF+LLG [Fig. 2] calculations of *nonequilibirum* dynamics of photoexcited electrons coupled to local magnetization. The central active region (CAR) consists of two layers of a 2D AF semicoductor, which are described by the top and bottom TB chains (as inspired by the quasi-1D structure of CrSBr [36–38]) hosting two orbitals, $c$(onduction) and $v$(alence), per site $i$. Electron spin densities (green arrows), $\langle \hat{\mathbf{s}}_{i_c}(t)\rangle$ and $\langle \hat{\mathbf{s}}_{i_v}(t)\rangle$, interact via $sd$ exchange [Eq. (10) and (11)] with classical LMM at the same site described by vector (red arrow) $\mathbf{M}_i(t)$ obeying the LLG Eq. (3). Electrons on $c$ and $v$ orbitals at the site $i$ interact via inter-orbital local Coulomb interaction of strength $U$ [Eq. (14)] which, when turned on $U > 0$, binds photoexcited electrons and holes into excitons [39, 40]. Both chains are attached to semi-infinite ideal NM leads modeled as 1D TB chains. Via such leads, any spin or charge current pumped within CAR by fsLP, or by excited magnons [41–43] persisting after fsLP ceases, is drained [Fig. 4] toward macroscopic reservoirs kept at the same Fermi energy $E_F$ (i.e., no bias voltage is applied between the leads). We also compute EM radiation, emitted by pumped local charge currents within the CAR, and analyze its frequency content in the THz range [Fig. 5].

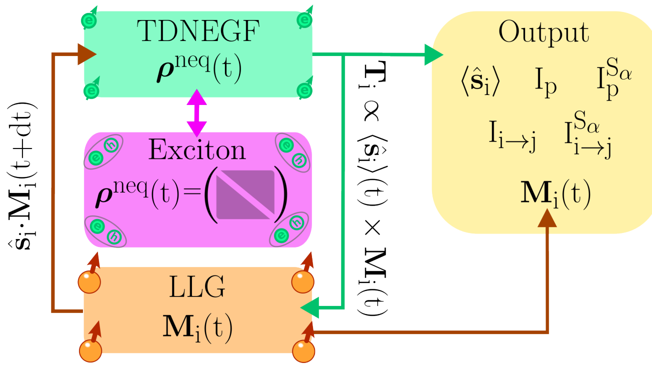


FIG. 2. Flowchart of TDNEGF+LLG self-consistent loop combining TDNEGF [62–64] (green box) computation [Eq. (4)] of time-dependent nonequilibrium density matrix $\rho^{\rm neq}(t)$ with LLG equation [56–58] updating (orange box) LMMs $\mathbf{M}_i(t)$. For this study, to the previously developed [65, 66] TDNEGF+LLG scheme, we add a computation (magenta box) employing [40] all off-diagonal elements of $\rho^{\rm neq}(t)$ in order to describe the binding of photoexcited conduction-band electrons and valence-band holes into excitons. The loop employs time step $\delta t = 0.1$ fs in both quantum (as required for numerical stability of TDNEGF calculations [62, 63, 65]) and classical LLG calculations. After each time step, we obtain time-dependent observables [Eqs. (1), (6), (7) and (17)] listed in the yellow box. In particular, STT is constructed from the expectation value of electron spin $\langle \hat{\mathbf{s}}_i(t)\rangle$ [Eq. (1)] and $\mathbf{M}_i(t)$ via Eq. (2).

the Landau-Lifshitz-Gilbert (LLG) equation [56] for localized magnetic moments (LMMs) viewed as classical (unit) vectors $\mathbf{M}_i(t)$ [Fig. 1]. While no effect of photoexcited electrons is explicitly included in the LLG equation, it has been conjectured that the configuration of LMMs can affect exciton energy in the case of CrSBr [3–5]. The agreement between such phenomenological models and experimentally excited magnon spectra implies that magnons can be approximately treated as classical spin waves [57, 58], despite challenges [59, 60] that AF materials pose for classical LLG treatment. We recall that in LLG description, magnons [24, 57, 58] emerge as collective excitations above a magnetically ordered ground state in which $\mathbf{M}_i(t)$ precess around a direction specified by magnetic anisotropy and/or an externally applied magnetic field [3–8]. The phase of precession $\mathbf{M}_i(t)$ of adjacent vectors varies harmonically in space over the magnon wavelength $\lambda$. However, microscopic understanding is lacking regarding what provides the initial "kick" for LLG dynamics to be initiated. Furthermore, excited magnons could imprint their signatures [41–43, 61] on currents flowing through 2D AF semiconductor, but their properties and usage as novel experimental probes remain unexplored.

In this Letter, we also employ the LLG equation, but we introduce the "kick" *microscopically* by self-consistently coupling LLG equation to computational quantum transport [67] of photoexcited electrons. Such electrons are described by the time-dependent nonequilibrium Green's functions (TDNEGF) formalism [62–64], as illustrated in Fig. 2. Thus, the TDNEGF+LLG framework [41, 65, 66, 68, 69] makes it possible to introduce into the LLG equation, in *numerically exact* fashion, the effect of photocurrent [70] ignited by fsLP. The photocurrent will become spin-polarized as it propagates through the magnetic environment created by LMMs. In addition, since LMMs within AF CAR in Fig. 1 will be noncollinear due to inevitable thermal fluctuations [71, 72] or applied magnetic field in experiments [3–5] that we also include [Eq. (10)], the nonequilibrium spin density

$$\langle \hat{\mathbf{s}}_{ia}\rangle(t) = {\rm Tr}_{\rm spin}[\rho^{\rm neq}(t)\sigma], \tag{1}$$

of photoexcited electrons will lead to nonzero spin-transfer torque (STT) [73–75] on the LMMs $\mathbf{M}_i$,

$$\mathbf{T}_i(t) = J_{sd}\left[\sum_{a=c,v}\langle \hat{\mathbf{s}}_{ia}\rangle(t)\right]\times\mathbf{M}_i(t). \tag{2}$$

The STT describes [73–75] how flowing electrons transfer spin angular momentum to local magnetization through $sd$ exchange interaction $J_{sd}$ [76]. Here $a = c, v$ labels each of two orbitals per site [Fig. 1]; $\sigma = (\hat{\sigma}_x, \hat{\sigma}_y, \hat{\sigma}_z)$ is the vector of the Pauli matrices; $\rho^{\rm neq}(t)$ is time-dependent nonequilibrium density matrix [62, 63, 77]; and trace $\mathrm{Tr}_{\rm spin}[\ldots]$ is over quantum states in the spin space only. Such microscopically computed STT is sent into the LLG equation,

$$\partial_t \mathbf{M}_i \;=\; -g_0 \mathbf{M}_i \times \mathbf{B}_i^{\rm eff} + \alpha_G \mathbf{M}_i \times \partial_t \mathbf{M}_i + \frac{g_0}{\mu_M} \mathbf{T}_i, \quad (3)$$

while dynamics of $\mathbf{M}_i(t)$ modifies the quantum Hamiltonian [Eq. (11)] of electrons within the loop in Fig. 2. This then establishes self-consistency between TDNEGF and LLG calculations, as initially photoexcited spin current, $I^{S_\alpha} = \mathrm{Tr}[\rho^{\rm neq}(t) \hat{I}^{S_\alpha}]$, will be modified by the dynamics of $\mathbf{M}_i(t)$; whereas their trajectories are, in turn, affected by updated spin current and STT $\mathbf{T}_i(t)$ exerted by it. In LLG Eq. (3) $g_0$ is gyromagnetic factor [56]; $\mu_M$ is the magnitude of LMMs [56]; $\mathbf{B}_i^{\rm eff} = -\frac{1}{\mu_M} \partial \mathcal{H} / \partial \mathbf{M}_i$ is effective magnetic field obtained from *classical* Hamiltonian $\mathcal{H}$ for LMMs [37, 78]; Gilbert damping is chosen as $\alpha_G = 0.01$, which is the typical value for Cr-based 2D magnets [78]; and we use shorthand notation $\partial_t \equiv \partial / \partial t$.

The fundamental quantity of quantum statistical mechanics is the density matrix. The time-dependent one-particle nonequilibrium density matrix, $\rho^{\rm neq}(t) = \hbar \mathbf{G}^<(t,t)/i$, can be expressed in terms of the lesser Green's function of TDNEGF formalism $G_{ii'}^{<,\sigma\sigma'}(t,t') = \frac{i}{\hbar} \langle \hat{c}^\dagger_{i'\sigma'}(t') \hat{c}_{i\sigma}(t) \rangle_{\rm nes}$ [62] where $\langle \ldots \rangle_{\rm nes}$ is the nonequilibrium statistical average [64]. We solve a matrix integro-differential equation [63]

$$i\hbar \partial_t \rho^{\rm neq} = [\mathbf{H}(t), \rho^{\rm neq}] + i \sum_{p=L,R} [\Pi_p(t) + \Pi_p^\dagger(t)], \quad (4)$$

for the time evolution of $\rho^{\rm neq}(t)$, where $\mathbf{H}(t)$ is the matrix representation of the *quantum* Hamiltonian of electrons. Equation (4) is an *exact* quantum master equation for the reduced density matrix of the AF CAR in Fig. 2 viewed as an open finite-size quantum system attached to macroscopic Fermi liquid reservoirs via semi-infinite normal metal (NM) leads. The NM leads, *not exploited* in experiments [3–9] thus far, are important technically within TDNEGF calculations in order to introduce continuous energy spectrum and dissipation effects [81], thereby guaranteeing that excited photocurrent and $\mathbf{M}_i(t)$ dynamics will eventually cease at some time after fsLP. Otherwise, in a closed quantum system [72] without a surrounding bath [71] one would find forever oscillating photocurrent, which is obviously unphysical. Furthermore, the leads allow us to analyze properties of charge and spin currents outflowing into them. Such currents could also offer novel experimental probe of excitons, magnons, and their interactions, as we confirm in Fig. 5. For this purpose, we use $\Pi_p(t)$ matrices

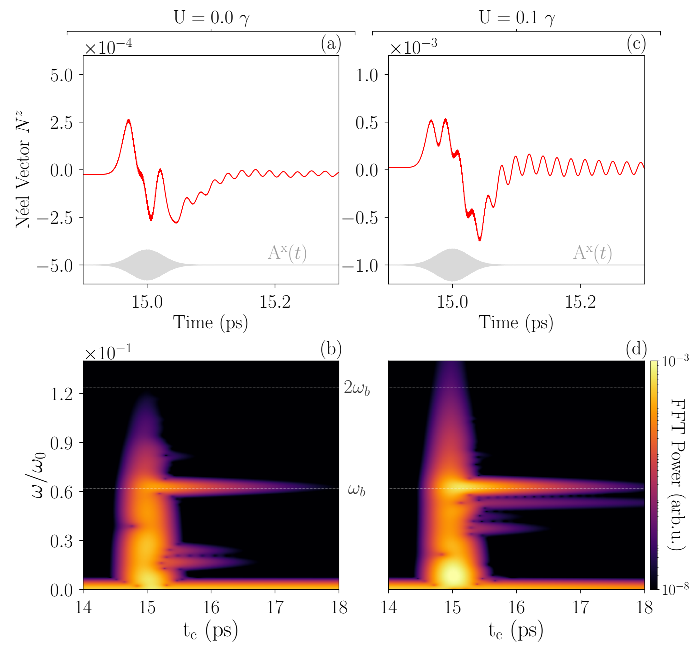


FIG. 3. Time dependence of the Néel vector, defined [Eq. (8)] for two monolayers of AF semiconductor CAR [Fig. 1] in: (a) the absence of excitons ($U = 0$); or (c) their presence induced by on-site Coulomb interaction [39, 40] $U = 0.1\gamma$ [Eq. (14)]. Panels (b) and (d) plot the corresponding power spectrum of windowed FFT [79, 80], $|N^y(t_c, \omega)|^2$, revealing frequencies and lifetime of magnons excited by STT from the photocurrent of conduction electrons in (a) or excitons in (b), respectively. Here $t_c$ denotes the central time of the Gaussian window [79, 80] used in FFT. Note that $\omega_b$ labels the frequency of the bright magnon, which corresponds to the same type of magnon in bilayer AF semiconductors observed in experiments of Refs. [3–5]. Gray curves on the bottom of panels (a) and (c) depict the vector potential $A^x(t)$ of fsLP.

$$\Pi_p(t) = \int_0^t dt_2 \, [\mathbf{G}^>(t,t_2) \Sigma_p^<(t_2,t) - \mathbf{G}^<(t,t_2) \Sigma_p^>(t_2,t)], \quad (5)$$

expressed in terms of the lesser and greater Green's functions [64] and the corresponding self-energies $\Sigma_p^{>,<}(t,t')$ [63], to obtain time-dependent charge

$$I_p(t) = \frac{e}{\hbar} \mathrm{Tr}\, [\Pi_p(t)], \quad (6)$$

and spin

$$I_p^{S_\alpha}(t) = \frac{e}{\hbar} \mathrm{Tr}\, [\hat{\sigma}_\alpha \Pi_p(t)], \quad (7)$$

currents outflowing into $p = L, R$ NM leads. Since the applied bias voltage between the left ($L$) and right ($R$) NM leads is identically zero in the setup of Fig. 1, all computed currents $I_p(t)$ and $I_p^{S_\alpha}(t)$ are solely due to *pumping* [41, 65, 68, 82–84] by (nonperiodic [82]) time-dependence of the CAR Hamiltonian. Note that we use

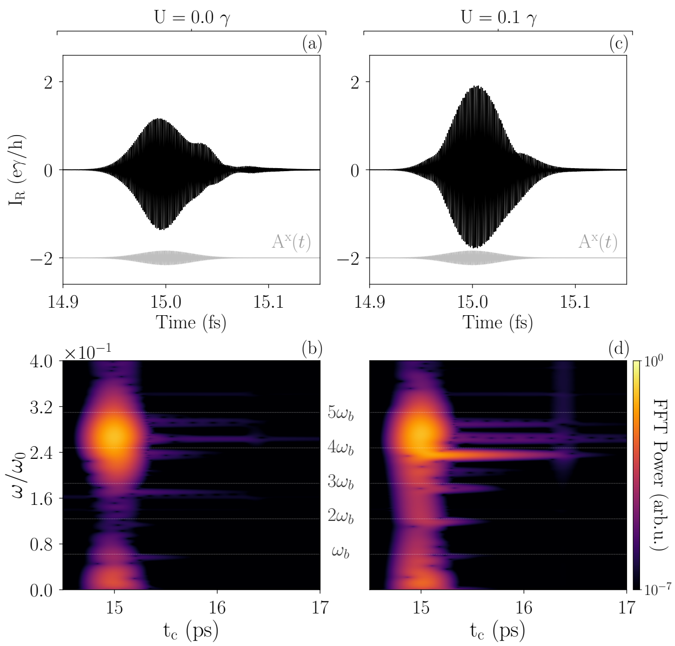


FIG. 4. Time-dependence of charge current $I_R(t)$ flowing into the right NM lead in Fig. 1 due to pumping [41–43] by excited magnons from Fig. 3 in: (a) the absence of excitons ($U = 0$); or (c) their presence induced by on-site Coulomb interaction $U = 0.1\gamma$ [Eq. (14)]. Panels (b) and (d) plot the corresponding power spectrum of windowed FFT [79, 80], $|I_R(t_c, \omega)|^2$. Gray curves on the bottom of panels (a) and (c) depict the vector potential $A^x(t)$ of fsLP.

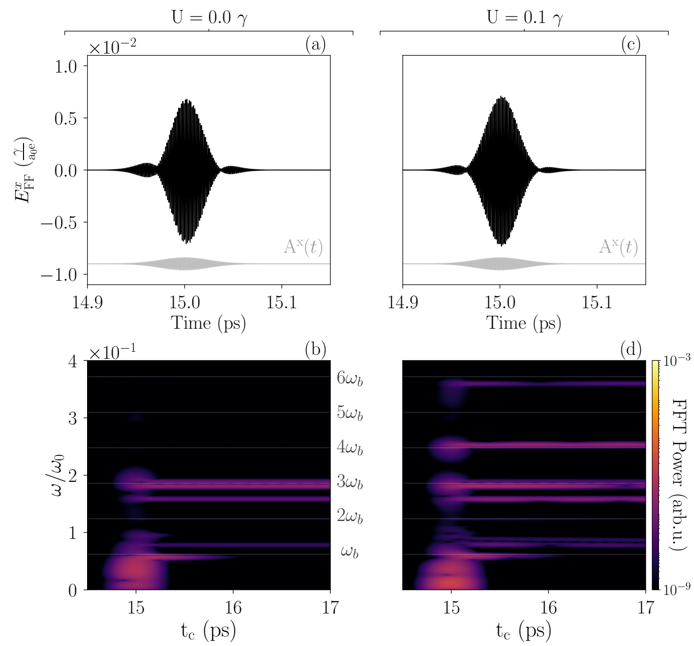


FIG. 5. Time-dependence of $E^x_{\rm FF}(t)$ the component of the electric field in the FF region of EM radiation emitted by bond charge currents [Eq. (17)] within the CAR of Fig. 1 in: (a) the absence of excitons ($U = 0$); or (c) their presence induced by on-site Coulomb interaction $U = 0.1\gamma$ [Eq. (14)]. Panels (b) and (d) plot the corresponding power spectrum of windowed FFT [79, 80], $|E^x_{\rm FF}(t_c, \omega)|^2$. Gray curves on the bottom of panels (a) and (c) depict the vector potential $A^x(t)$ of fsLP.

the same units for charge and spin currents, defined as $I_p = I_p^\uparrow + I_p^\downarrow$ and $I_p^{S_\alpha} = I_p^\uparrow - I_p^\downarrow$, in terms of spin-resolved charge currents $I_p^\sigma$. In our convention, positive current in NM lead $p$ means charge or spin current is flowing out of that NM lead.

Let us recall that the problem of how STT excites uniform motion of all LMMs [i.e., of their macrospin $\mathbf{M}(t) = \sum_i \mathbf{M}_i(t)$] vs. their nonuniform motion like magnons was analyzed long ago [85] for conventional metallic ferromagnets, as well as recently for AF insulators [69, 86], with focus on threshold injected current value [33, 87] for magnons to occur. Our setup in Fig. 2 is different from those studies, as no current is injected from an external circuit. Instead, photocurrent is excited within the AF semiconductor CAR by fsLP, and can eventually exit into the NM leads. In addition to photocurrent of conduction electrons, we also consider photocurrent of excitons generated by Coulomb interaction, which binds conduction-band electrons with valence-band holes. To capture such binding, we employ a time-dependent mean-field theory (tMFT) [39, 40] of inter-orbital Coulomb interaction term [Eq. (14)]. For this purpose, we exploit [40] the off-diagonal elements of $\rho^{\rm neq}(t)$, that we naturally construct within the TDNEGF part [62, 63] of TDNEGF+LLG self-consistent loop [41, 65, 66, 68, 69]. In other words, for the study presented here, the previously developed [41, 65, 66, 68, 69, 88] TDNEGF+LLG framework is amended with modeling of excitonic effects. Details of our quantum Hamiltonian for the electronic subsystem, $\hat{H}$, and the classical one, $\mathcal{H}$, for the subsystem of LMMs, together with explanations of tMFT and electromagnetic radiation (EM) calculations via the Jefimenko equations [82, 89–94], are provided in End Matter.

*Results and Discussion.*—We first recall the definition [3–5, 8] of the Néel vector

$$\mathbf{N} \equiv (N^x, N^y, N^z) = \frac{1}{2N} \sum_{i\in 1, j\in 2} \big(\mathbf{M}_i - \mathbf{M}_j\big), \tag{8}$$

between two monolayers of AF semiconductor, where in equilibrium $\mathbf{N}(t=0) \equiv (2,0,0)$. Out of equilibrium, as initiated by fsLP, the Néel vector starts evolving in time [Figs. 3(a) and 3(c)]. Somewhat surprisingly and also observed experimentally [13], this evolution starts without substantial delay regarding fsLP, even though LMMs are slower than electrons [71]. Because the magnon frequency spectrum encoded in $N^z(t)$ could be changing within different time frames, we apply windowed (or short-time) Fast Fourier transform (FFT) [79, 80, 95, 96]. For example, magnons get excited around $t_c \simeq 15$ ps in Fig. 3(b), and subsequently they decay [23, 27] because of Gilbert damping $\alpha_G$ in Eq. (3). Furthermore, because of explicitly introduced electrons via TDNEGF calculations, additional *nonlocal* damping [66, 97–102] is introduced into Eq. (3) via the STT term $\mathbf{T}_i(t)$. Due to such decay, excited magnons vanish at around $t_c \simeq 18$ ps in Fig. 3(b). For such signals—appearing also in many other scientific disciplines (such as electroencephalography [80] or speech analysis)—it is advantageous to perform windowed FFT over successive time intervals. For this purpose, we employ Gaussian as the window function,

$$X(t_c, \omega) = \frac{1}{\lambda\sigma(2\pi)^{3/2}} \int_0^\infty dt\, X(t) e^{i\omega t} e^{-(t-t_c)^2/2(\lambda\sigma)^2}, \quad (9)$$

which makes it possible to extract time-frequency content from signals whose oscillations are localized in a finite time frame. Here, $t_c$ is the centroid of the Gaussian, serving as the abscissa of panels (b) and (d) within each of Figs. 3–5 analyzing $X(t) = N^\alpha(t), I_R(t), E^x_{\rm FF}(t)$ as the signal, respectively. Here, $\sigma$ specifies the width of the Gaussian and $\lambda$ is a parameter controlling the resolution. For example, greater values of $\lambda\sigma$ yield better resolution in the time domain, while smaller values yield improved resolution in the frequency domain, where the frequency and time resolution satisfy a Heisenberg-like uncertainty relation [79, 80]. Windowed FFT of the Néel vector produces $N^z(\omega, t_c)$, whose power spectrum in Figs. 3(b) and 3(d) reveals excitation of the so-called "bright magnon" at the frequency $\omega_b$. Thus, our TDNEGF+LLG theory explains fully microscopically the same "bright magnon" observed experimentally [3–5, 8]. In the presence of excitons due to nonzero $U$, we find longer lifetime of excited magnons in Fig. 3(d). Both Figs. 3(b) and 3(d) also show short (for $U = 0$) vs. longer (for $U \neq 0$) living magnons, respectively, that are excited at frequencies below $\omega_b$. We confirm in Fig. S1(a) of the Supplemental Material (SM) [103] that such magnons are a direct consequence of $J_{sd} \neq 0$.

The excited magnons will introduce the second nonequlibrium drive into the subsystem of electrons. Such a time-dependent drive can lead to *pumping* [41–43, 61] of electronic spin and charge currents. They can be differentiated from currents pumped [70] by fsLP, as the first nonequilibirum drive, by their specific frequency content. We compute charge current $I_R(t)$ [Figs. 4(a) and 4(c)] pumped in the right NM lead, and perform windowed FFT on it to obtain $|I_R(t_c, \omega)|^2$ and plot it [Figs. 4(b) and 4(d)] in the same frequency range where magnons are found in Fig. 3. This power spectrum contains peaks at $\omega_b$, meaning that by attaching an additional external circuit to recent experiments and by analyzing pumped current into that circuit, one could confirm optical excitations of magnons. Note that pumped current is also a sensitive probe for the formation of excitons, as in $U \neq 0$ case long-lived high harmonic generation (HHG) emerges in Fig. 4(d).

Finally, we examine EM radiation that will be emitted by time-dependent local (or bond [104]) charge currents $I_{ia\to jb}(t)$ [Eq. (17)] within AF semiconductor CAR in Fig. 1. Note that EM radiation emitted by ultrafast-light-driven magnetic materials and their heterostructures is routinely used [105–108] in spintronic experiments as a probe of coupled spin-charge dynamics [82, 93, 94, 109] of such far-from-equilibrium systems. We compute the $x$-component $E^x_{\rm FF}(\mathbf{r}, t)$ of the electric field of EM radiation in the far-field (FF) region—where radiation decays as $\sim 1/r$, such as by using $\mathbf{r}_0 = (5a, 0, 1000a)$—via the Jefimenko [89, 91] Eq. (16) using $I_{ia\to jb}(t)$ as the source [71, 92]. The windowed FFT of $E^x_{\rm FF}(\mathbf{r}_0, t)$ in Figs. 5(a) and 5(c) yields $E^x_{\rm FF}(\mathbf{r}_0, t_c, \omega)$ whose power spectrum is plotted in Figs. 5(b) and 5(d), respectively. Similarly to $|I_R(t_c, \omega)|^2$, the power spectrum $|E^x_{\rm FF}(t_c, \omega)|^2$ contains an imprint of excited "bright magnon", as well as HHG signaling [Fig. 5(d)] the presence of exciton-magnon interactions. Note that the frequency content of EM radiation related to magnons is in the range of: THz in Fig. 5 for our model; sub-THz for $CrI_3$ in Ref. [13]; and GHz for CrSBr in Ref. [5].

*Conclusions and Outlook.*—Using computational time-dependent quantum transport [62, 63], extended [39, 40] to include binding of photoexcited electrons and holes into excitons, we demonstrate that the microscopic mechanism behind recent experimental observations [3–5, 8, 13, 45] of optical excitation of "bright magnon" in bilayer 2D AF semiconductors is a *nonequilibrium spintronic effect of spin torque type* [73, 110]. This approach displaces the need for a phenomenological picture of "impulsive perturbation" [5, 13], invoked within the classical LLG equation alone to interpret these experiments, while revealing additional signatures [Figs. 4 and 5] of magnons and their interaction with excitons that could be exploited in future experiments. We note that very recent experiments [5] on CrSBr have also observed HHG of magnons at frequencies $n\omega_b$, with $n$ reaching surprisingly large $n \gtrsim 20$. In contrast, our theory [Fig. 3] reproduces only "bright magnon" at frequency $\omega_b$. Although the LLG equation is nonlinear and can, in principle, capture [24, 60] magnon-magnon interactions (made important [23] by experimentally induced noncollinearity of LMMs within CrSBr [5]) as one of the key ingredients [111] for large $n$, it seems that LLG dynamics on its own is insufficient. Another hint is offered by Fig. S1(c) in the SM where we find that increasing $J_{sd}$ to an unrealistically large value (i.e., ten times larger than used in Figs. 3–5, as a parameter which is difficult to extract from first-principles calculations [40]) leads to HHG but at noninteger $n$. We anticipate that adding quantum corrections [112, 113] to the LLG equation, as often required for AF materials [59, 60, 111]; and/or by treating excitons beyond tMFT— which can be achieved within TDNEGF formalism by including additional self-energies in Eq. (4), and then systematically improving them [39, 64, 114, 115]—could explain the experimentally observed [5] HHG of magnons and the role of many-body interactions with excitons in this process. We relegate such extensions of the TDNEGF+LLG framework to future studies.

J. V.-M. and Y. R. were supported by the University of Delaware (UD) Research Foundation Strategic Initiative Award. Y. R. and B. K. N. were supported by the US National Science Foundation (NSF) through the UD Materials Research Science and Engineering Center (MRSEC), DMR-2011824. The supercomputing time was provided by DARWIN (Delaware Advanced Research Workforce and Innovation Network), which is supported by NSF Grant No. MRI-1919839.

* bnikolic@udel.edu


[1] M. Gibertini, M. Koperski, A. F. Morpurgo, and K. S. Novoselov, Magnetic 2D materials and heterostructures, Nat. Nanotechnol. **14**, 408 (2019).

[2] J. T. Gish, D. Lebedev, T. W. Song, V. K. Sangwan, and M. C. Hersam, Van der Waals opto-spintronics, Nat. Electron. **7**, 336 (2024).

[3] Y. J. Bae, J. Wang, A. Scheie, J. Xu, D. G. Chica, G. M. Diederich, J. Cenker, M. E. Ziebel, Y. Bai, H. Ren, C. R. Dean, M. Delor, X. Xu, X. Roy, A. D. Kent, and X. Zhu, Exciton-coupled coherent magnons in a 2D semiconductor, Nature **609**, 282 (2022).

[4] G. M. Diederich, J. Cenker, Y. Ren, J. Fonseca, D. G. Chica, Y. J. Bae, X. Zhu, X. Roy, T. Cao, D. Xiao, and X. Xu, Tunable interaction between excitons and hybridized magnons in a layered semiconductor, Nat. Nanotechnol. **18**, 23 (2022).

[5] G. M. Diederich, M. Nguyen, J. Cenker, J. Fonseca, S. Pumulo, Y. J. Bae, D. G. Chica, X. Roy, X. Zhu, D. Xiao, Y. Ren, and X. Xu, Exciton dressing by extreme nonlinear magnons in a layered semiconductor, Nat. Nanotechnol. **20**, 617 (2025).

[6] T. Wang, D. Zhang, S. Yang, Z. Lin, Q. Chen, J. Yang, Q. Gong, Z. Chen, Y. Ye, and W. Liu, Magnetically-dressed CrSBr exciton-polaritons in ultrastrong coupling regime, Nat. Commun. **14**, 5966 (2023).

[7] F. Dirnberger, J. Quan, R. Bushati, G. M. Diederich, M. Florian, J. Klein, K. Mosina, Z. Sofer, X. Xu, A. Kamra, *et al.*, Magneto-optics in a van der Waals magnet tuned by self-hybridized polaritons, Nature **620**, 533 (2023).

[8] Y. Sun, F. Meng, C. Lee, A. Soll, H. Zhang, R. Ramesh, J. Yao, Z. Sofer, and J. Orenstein, Dipolar spin wave packet transport in a van der Waals antiferromagnet, Nat. Phys. **20**, 794 (2024).

[9] B. Datta, P. C. Adak, S. Yu, A. Valiyaparambil Dharmapalan, S. J. Hall, A. Vakulenko, F. Komissarenko, E. Kurganov, J. Quan, W. Wang, *et al.*, Magnon-mediated exciton–exciton interaction in a van der Waals antiferromagnet, Nat. Mater. **24**, 1027 (2025).

[10] C. A. Belvin, E. Baldini, I. O. Ozel, D. Mao, H. C. Po, C. J. Allington, S. Son, B. H. Kim, J. Kim, I. Hwang, J. H. Kim, J.-G. Park, T. Senthil, and N. Gedik, Exciton-driven antiferromagnetic metal in a correlated van der Waals insulator, Nat. Commun. **12**, 4837 (2021).

[11] Z. Wang, X.-X. Zhang, Y. Shiomi, T.-h. Arima, N. Nagaosa, Y. Tokura, and N. Ogawa, Exciton-magnon splitting in the van der Waals antiferromagnet $MnPS_3$ unveiled by second-harmonic generation, Phys. Rev. Res. **5**, L042032 (2023).

[12] M. Onga, Y. Sugita, T. Ideue, Y. Nakagawa, R. Suzuki, Y. Motome, and Y. Iwasa, Antiferromagnet–semiconductor van der Waals heterostructures: Interlayer interplay of exciton with magnetic ordering, Nano Letters **20**, 4625 (2020).

[13] X.-X. Zhang, L. Li, D. Weber, J. Goldberger, K. F. Mak, and J. Shan, Gate-tunable spin waves in antiferromagnetic atomic bilayers, Nat. Mater. **19**, 838 (2020).

[14] D. Bossini, M. Pancaldi, L. Soumah, M. Basini, F. Mertens, M. Cinchetti, T. Satoh, O. Gomonay, and S. Bonetti, Ultrafast amplification and nonlinear magnetoelastic coupling of coherent magnon modes in an antiferromagnet, Phys. Rev. Lett. **127**, 077202 (2021).

[15] Studies [16–22] of exciton-magnon coupled systems in the 1960s and 1970s were largely motivated by absorption spectra of particular three-dimensional AF insulators like $MnF_2$.

[16] Y. Tanabe, T. Moriya, and S. Sugano, Magnon-induced electric dipole transition moment, Phys. Rev. Lett. **15**, 1023 (1965).

[17] D. D. Sell, R. L. Greene, and R. M. White, Optical exciton-magnon absorption in $MnF_2$, Phys. Rev. **158**, 489 (1967).

[18] S. Freeman and J. J. Hopfield, Exciton-magnon interaction in magnetic insulators, Phys. Rev. Lett. **21**, 910 (1968).

[19] J. B. Parkinson, Theory of localized magnons and magnon-exciton interactions in antiferromagnetic perovskites, J. Appl. Phys. **40**, 993 (1969).

[20] I. G. Gochev, Bound magnon-exciton states, Theor. Math. Phys. **22**, 290 (1975).

[21] A. A. Loginov and V. A. Popov, Exciton–magnon coupling in antiferromagnets and its influence on the energy spectrum of excitons, Sov. J. Low Temp. Phys. **7**, 43 (1981).

[22] V. V. Gorbach, On a possible multimagnon generation mechanism under exciton light absorption in antiferromagnetics, physica status solidi (b) **149**, K49 (1988).

[23] M. E. Zhitomirsky and A. L. Chernyshev, Colloquium: Spontaneous magnon decays, Rev. Mod. Phys. **85**, 219 (2013).

[24] S. Zheng, Z. Wang, Y. Wang, F. Sun, Q. He, P. Yan, and H. Yuan, Tutorial: Nonlinear magnonics, J. Appl. Phys. **134** (2023).

[25] O. Johansen, A. Kamra, C. Ulloa, A. Brataas, and R. A. Duine, Magnon-mediated indirect exciton condensation through antiferromagnetic insulators, Phys. Rev. Lett. **123**, 167203 (2019).

[26] C. Meineke, J. Schlosser, M. Zizlsperger, M. Liebich, N. Nilforoushan, K. Mosina, S. Terres, A. Chernikov, Z. Sofer, M. A. Huber, *et al.*, Ultrafast exciton dynamics in the atomically thin van der Waals magnet CrSBr, Nano Lett. **24**, 4101 (2024).

[27] B. Flebus, D. Grundler, B. Rana, Y. Otani, I. Barsukov, A. Barman, G. Gubbiotti, P. Landeros, J. Akerman, U. Ebels, *et al.*, The 2024 magnonics roadmap, J. Phys.:

Condens. Matter **36**, 363501 (2024).

[28] P. Pirro, V. I. Vasyuchka, A. A. Serga, and B. Hillebrands, Advances in coherent magnonics, Nat. Rev. Mater. **6**, 1114 (2021).

[29] A. De, A. Lentfert, L. Scheuer, B. Stadtmüller, G. von Freymann, M. Aeschlimann, and P. Pirro, Coherent and incoherent magnons induced by strong ultrafast demagnetization in thin permalloy films, Phys. Rev. B **109**, 024422 (2024).

[30] J. R. Hortensius, D. Afanasiev, M. Matthiesen, R. Leenders, R. Citro, A. V. Kimel, R. V. Mikhaylovskiy, B. A. Ivanov, and A. D. Caviglia, Coherent spin-wave transport in an antiferromagnet, Nat. Phys. **17**, 1001 (2021).

[31] A. Chumak, V. Vasyuchka, A. Serga, and B. Hillebrands, Magnon spintronics, Nat. Phys. **11**, 453 (2015).

[32] A. V. Chumak, P. Kabos, M. Wu, C. Abert, C. Adelmann, A. O. Adeyeye, J. Akerman, F. G. Aliev, A. Anane, A. Awad, *et al.*, Advances in magnetics roadmap on spin-wave computing, IEEE Transactions on Magnetics **58**, 1 (2022).

[33] R. Lebrun, A. Ross, S. A. Bender, A. Qaiumzadeh, L. Baldrati, J. Cramer, A. Brataas, R. A. Duine, and M. Kläui, Tunable long-distance spin transport in a crystalline antiferromagnetic iron oxide, Nature **561**, 222 (2018).

[34] R. Hisatomi, A. Osada, Y. Tabuchi, T. Ishikawa, A. Noguchi, R. Yamazaki, K. Usami, and Y. Nakamura, Bidirectional conversion between microwave and light via ferromagnetic magnons, Phys. Rev. B **93**, 174427 (2016).

[35] N. Lauk, N. Sinclair, S. Barzanjeh, J. P. Covey, M. Saffman, M. Spiropulu, and C. Simon, Perspectives on quantum transduction, Quantum Sci. Technol. **5**, 020501 (2020).

[36] J. Klein, B. Pingault, M. Florian, M.-C. Heißenbüttel, A. Steinhoff, Z. Song, K. Torres, F. Dirnberger, J. B. Curtis, M. Weile, A. Penn, T. Deilmann, R. Dana, R. Bushati, J. Quan, J. Luxa, Z. Sofer, A. Alù, V. M. Menon, U. Wurstbauer, M. Rohlfing, P. Narang, M. Lončar, and F. M. Ross, The bulk van der Waals layered magnet CrSBr is a quasi-1D material, ACS Nano **17**, 5316 (2023).

[37] A. Scheie, M. Ziebel, D. G. Chica, Y. J. Bae, X. Wang, A. I. Kolesnikov, X. Zhu, and X. Roy, Spin waves and magnetic exchange Hamiltonian in CrSBr, Adv. Sci. **9**, 2202467 (2022).

[38] Z.-H. Cui, A. J. Millis, and D. R. Reichman, Theory of interaction-induced charge order in CrSBr, Phys. Rev. B **111**, 245155 (2025).

[39] Y. Murakami, M. Schüler, S. Takayoshi, and P. Werner, Ultrafast nonequilibrium evolution of excitonic modes in semiconductors, Phys. Rev. B **101**, 035203 (2020).

[40] G. Cistaro, M. Malakhov, J. J. Esteve-Paredes, A. J. Uría-Álvarez, R. E. F. Silva, F. Martín, J. J. Palacios, and A. Picón, Theoretical approach for electron dynamics and ultrafast spectroscopy (EDUS), J. Chem. Theory Comput. **19**, 333 (2022).

[41] A. Suresh, U. Bajpai, and B. K. Nikolić, Magnon-driven chiral charge and spin pumping and electron-magnon scattering from time-dependent quantum transport combined with classical atomistic spin dynamics, Phys. Rev. B **101**, 214412 (2020).

[42] M. Evelt, H. Ochoa, O. Dzyapko, V. E. Demidov, A. Yurgens, J. Sun, Y. Tserkovnyak, V. Bessonov, A. B. Rinkevich, and S. O. Demokritov, Chiral charge pumping in graphene deposited on a magnetic insulator, Phys. Rev. B **95**, 024408 (2017).

[43] C. Ciccarelli, K. M. D. Hals, A. Irvine, V. Novak, Y. Tserkovnyak, H. Kurebayashi, A. Brataas, and A. Ferguson, Magnonic charge pumping via spin–orbit coupling, Nat. Nanotechnol. **10**, 50 (2015).

[44] D. Afanasiev, J. R. Hortensius, M. Matthiesen, S. Mañas-Valero, M. Šiškins, M. Lee, E. Lesne, H. S. J. van der Zant, P. G. Steeneken, B. A. Ivanov, E. Coronado, and A. D. Caviglia, Controlling the anisotropy of a van der Waals antiferromagnet with light, Sci. Adv. **7**, eabf3096 (2021).

[45] C. J. Allington, C. A. Belvin, U. F. P. Seifert, M. Ye, T. Tai, E. Baldini, S. Son, J. Kim, J. Park, J.-G. Park, L. Balents, and N. Gedik, Distinct optical excitation mechanisms of a coherent magnon in a van der Waals antiferromagnet, Phys. Rev. Lett. **134**, 066903 (2025).

[46] F. Reyes-Osorio and B. K. Nikolić, Bringing light into the Landau-Lifshitz-Gilbert equation: Consequences of its fractal non-Markovian memory kernel for optically induced magnetic inertia and magnons, arXiv:2504.17769 (2025).

[47] U. F. P. Seifert, M. Ye, and L. Balents, Ultrafast optical excitation of magnetic dynamics in van der Waals magnets: Coherent magnons and BKT dynamics in $NiPS_3$, Phys. Rev. B **105**, 155138 (2022).

[48] T. Satoh, S.-J. Cho, R. Iida, T. Shimura, K. Kuroda, H. Ueda, Y. Ueda, B. A. Ivanov, F. Nori, and M. Fiebig, Spin oscillations in antiferromagnetic NiO triggered by circularly polarized light, Phys. Rev. Lett. **105**, 077402 (2010).

[49] C. Tzschaschel, K. Otani, R. Iida, T. Shimura, H. Ueda, S. Günther, M. Fiebig, and T. Satoh, Ultrafast optical excitation of coherent magnons in antiferromagnetic NiO, Phys. Rev. B **95**, 174407 (2017).

[50] E. Rongione, O. Gueckstock, M. Mattern, O. Gomonay, H. Meer, C. Schmitt, R. Ramos, T. Kikkawa, M. Mičica, E. Saitoh, J. Sinova, H. Jaffrès, J. Mangeney, S. T. B. Goennenwein, S. Geprägs, T. Kampfrath, M. Kläui, M. Bargheer, T. S. Seifert, S. Dhillon, and R. Lebrun, Emission of coherent THz magnons in an antiferromagnetic insulator triggered by ultrafast spin–phonon interactions, Nat. Commun. **14**, 1818 (2023).

[51] U. F. P. Seifert and L. Balents, Optical excitation of magnons in an easy-plane antiferromagnet: Application to $Sr_2IrO_4$, Phys. Rev. B **100**, 125161 (2019).

[52] Z. Chen and L.-W. Wang, Role of initial magnetic disorder: A time-dependent ab initio study of ultrafast demagnetization mechanisms, Sci. Adv. **5**, eaau800 (2019).

[53] A. Kudlis, M. Kazemi, Y. Zhumagulov, H. Schrautzer, A. I. Chernov, P. F. Bessarab, I. V. Iorsh, and I. A. Shelykh, All-optical magnetization control in $CrI_3$ monolayers: A microscopic theory, Phys. Rev. B **108**, 094421 (2023).

[54] T. Olsen, Unified treatment of magnons and excitons in monolayer $CrI_3$ from many-body perturbation theory, Phys. Rev. Lett. **127**, 166402 (2021).

[55] H. Y. Yuan, S. Zheng, Q. Y. He, J. Xiao, and R. A. Duine, Unconventional magnon excitation by off-resonant microwaves, Phys. Rev. B **103**, 134409 (2021).

[56] R. F. L. Evans, W. J. Fan, P. Chureemart, T. A. Ostler, M. O. A. Ellis, and R. W. Chantrell, Atomistic spin

model simulations of magnetic nanomaterials, J. Phys. Condens. Matter **26**, 103202 (2014).

[57] S.-K. Kim, Micromagnetic computer simulations of spin waves in nanometre-scale patterned magnetic elements, J. Phys. D: Appl. Phys. **43**, 264004 (2010).

[58] L. Moreels, I. Lateur, D. D. Gusem, J. Mulkers, J. Maes, M. V. Milošević, J. Leliaert, and B. V. Waeyenberge, mumax+: Extensible gpu-accelerated micromagnetics and beyond, arXiv:2411.18194 (2024).

[59] F. Garcia-Gaitan and B. K. Nikolić, Fate of entanglement in magnetism under Lindbladian or non-Markovian dynamics and conditions for their transition to Landau-Lifshitz-Gilbert classical dynamics, Phys. Rev. B **109**, L180408 (2024).

[60] F. Garcia-Gaitan, A. Kefayati, J. Q. Xiao, and B. K. Nikolić, Magnon spectrum of altermagnets beyond linear spin wave theory: Magnon-magnon interactions via time-dependent matrix product states versus atomistic spin dynamics, Phys. Rev. B **111**, L020407 (2025).

[61] A. Kapelrud and A. Brataas, Spin pumping and enhanced Gilbert damping in thin magnetic insulator films, Phys. Rev. Lett. **111**, 097602 (2013).

[62] B. Gaury, J. Weston, M. Santin, M. Houzet, C. Groth, and X. Waintal, Numerical simulations of time-resolved quantum electronics, Phys. Rep. **534**, 1 (2014).

[63] B. S. Popescu and A. Croy, Efficient auxiliary-mode approach for time-dependent nanoelectronics, New J. Phys. **18**, 093044 (2016).

[64] G. Stefanucci and R. Van Leeuwen, *Nonequilibrium many-body theory of quantum systems: A modern introduction* (Cambridge University Press, 2025).

[65] M. D. Petrović, B. S. Popescu, U. Bajpai, P. Plecháč, and B. K. Nikolić, Spin and charge pumping by a steady or pulse-current-driven magnetic domain wall: A self-consistent multiscale time-dependent quantum-classical hybrid approach, Phys. Rev. Appl. **10**, 054038 (2018).

[66] U. Bajpai and B. K. Nikolić, Time-retarded damping and magnetic inertia in the Landau-Lifshitz-Gilbert equation self-consistently coupled to electronic time-dependent nonequilibrium green functions, Phys. Rev. B **99**, 134409 (2019).

[67] X. Waintal, M. Wimmer, A. Akhmerov, C. Groth, B. K. Nikolić, M. Istas, T. Örn Rosdahl, and D. Varjas, Computational quantum transport, arXiv:2407.16257 (2024).

[68] M. D. Petrović, U. Bajpai, P. Plecháč, and B. K. Nikolić, Annihilation of topological solitons in magnetism with spin-wave burst finale: Role of nonequilibrium electrons causing nonlocal damping and spin pumping over ultrabroadband frequency range, Phys. Rev. B **104**, L020407 (2021).

[69] A. Suresh, U. Bajpai, M. D. Petrović, H. Yang, and B. K. Nikolić, Magnon- versus electron-mediated spin-transfer torque exerted by spin current across an antiferromagnetic insulator to switch the magnetization of an adjacent ferromagnetic metal, Phys. Rev. Appl. **15**, 034089 (2021).

[70] U. Bajpai, B. S. Popescu, P. Plecháč, B. K. Nikolić, L. E. F. F. Torres, H. Ishizuka, and N. Nagaosa, Spatio-temporal dynamics of shift current quantum pumping by femtosecond light pulse, J. Phys.: Mater. **2**, 025004 (2019).

[71] A. Suresh and B. K. Nikolić, Quantum classical approach to spin and charge pumping and the ensuing radiation in terahertz spintronics: Example of the ultrafast light-driven Weyl antiferromagnet $Mn_3Sn$, Phys. Rev. B **107**, 174421 (2023).

[72] S. Ghosh, F. Freimuth, O. Gomonay, S. Blügel, and Y. Mokrousov, Driving spin chirality by electron dynamics in laser-excited antiferromagnets, Commun. Phys. **5**, 69 (2022).

[73] D. Ralph and M. Stiles, Spin transfer torques, J. Magn. Magn. Mater. **320**, 1190 (2008).

[74] B. K. Nikolić, K. Dolui, M. Petrović, P. Plecháč, T. Markussen, and K. Stokbro, First-principles quantum transport modeling of spin-transfer and spin-orbit torques in magnetic multilayers, in *Handbook of Materials Modeling*, edited by W. Andreoni (Springer, Cham, 2018) pp. 1–35, arXiv:1801.05793.

[75] K. D. Belashchenko, A. A. Kovalev, and M. van Schilfgaarde, First-principles calculation of spin-orbit torque in a Co/Pt bilayer, Phys. Rev. Mater. **3**, 011401 (2019).

[76] R. L. Cooper and E. A. Uehling, Ferromagnetic resonance and spin diffusion in supermalloy, Phys. Rev. **164**, 662 (1967).

[77] U. Bajpai and B. K. Nikolić, Spintronics meets nonadiabatic molecular dynamics: Geometric spin torque and damping on dynamical classical magnetic texture due to an electronic open quantum system, Phys. Rev. Lett. **125**, 187202 (2020).

[78] D. L. Esteras, A. Rybakov, A. M. Ruiz, and J. J. Baldoví, Magnon straintronics in the 2D van der Waals ferromagnet CrSBr from first-principles, Nano Lett. **22**, 8771 (2022).

[79] W. H. Press, S. A. Teukolsky, W. T. Vetterling, and B. P. Flannery, *Numerical Recipes: The Art of Scientific Computing* (Cambridge University Press, Cambridge, 2007).

[80] M. X. Cohen, *Analyzing Neural Time Series Data: Theory and Practice* (The MIT Press, Cambridge,, 2014).

[81] J. Varela-Manjarres and B. K. Nikolić, High-harmonic generation in spin and charge current pumping at ferromagnetic or antiferromagnetic resonance in the presence of spin-orbit coupling, J. Phys. Mater. **6**, 045001 (2023).

[82] J. Varela-Manjarres, A. Kefayati, M. B. Jungfleisch, J. Q. Xiao, and B. K. Nikolić, Charge and spin current pumping by ultrafast demagnetization dynamics, Phys. Rev. B **110**, L060410 (2024).

[83] Y. Tserkovnyak, A. Brataas, G. E. Bauer, and B. I. Halperin, Nonlocal magnetization dynamics in ferromagnetic heterostructures, Rev. Mod. Phys. **77**, 1375 (2005).

[84] A. Abbout, J. Weston, X. Waintal, and A. Manchon, Cooperative charge pumping and enhanced skyrmion mobility, Phys. Rev. Lett. **121**, 257203 (2018).

[85] A. Brataas, Y. Tserkovnyak, and G. E. W. Bauer, Current-induced macrospin versus spin-wave excitations in spin valves, Phys. Rev. B **73**, 014408 (2006).

[86] M. W. Daniels, W. Guo, G. M. Stocks, D. Xiao, and J. Xiao, Spin-transfer torque induced spin waves in antiferromagnetic insulators, New J. Phys. **17**, 103039 (2015).

[87] Y. Kajiwara, K. Harii, S. Takahashi, J. Ohe, K. Uchida, M. Mizuguchi, H. Umezawa, H. Kawai, K. Ando, K. Takanashi, S. Maekawa, and E. Saitoh, Transmission of electrical signals by spin-wave interconversion in a magnetic insulator, Nature **464**, 262 (2010).

[88] https://wiki.physics.udel.edu/qttg/Download_Research_Software_by_QTTG.

[89] O. D. Jefimenko, *Electricity and Magnetism* (Appleton Century-Crofts, New York, 1966).

[90] D. J. Griffiths and M. A. Heald, Time-dependent generalizations of the Biot–Savart and Coulomb laws, Am. J. Phys. **59**, 111 (1991).

[91] K. T. McDonald, The relation between expressions for time-dependent electromagnetic fields given by Jefimenko and by Panofsky and Phillips, Am. J. Phys. **65**, 1074 (1997).

[92] M. Ridley, L. Kantorovich, R. van Leeuwen, and R. Tuovinen, Quantum interference and the time-dependent radiation of nanojunctions, Phys. Rev. B **103**, 115439 (2021).

[93] A. Kefayati and B. K. Nikolić, Origins of electromagnetic radiation from spintronic terahertz emitters: A time-dependent density functional theory plus jefimenko equations approach, Phys. Rev. Lett. **133**, 136704 (2024).

[94] F. Foggetti and P. M. Oppeneer, Quantitative modeling of spintronic terahertz emission due to ultrafast spin transport, Phys. Rev. Appl. **23**, 014067 (2025).

[95] M. Udono, K. Sugimoto, T. Kaneko, and Y. Ohta, Excitonic effects on high-harmonic generation in Mott insulators, Phys. Rev. B **105**, L241108 (2022).

[96] E. B. Molinero, B. Amorim, M. Malakhov, G. Cistaro, Álvaro Jiménez-Galán, A. Picón, P. San-José, M. Ivanov, and R. E. F. Silva, Subcycle dynamics of excitons under strong laser fields, Sci. Adv. **10**, eadn6985 (2024).

[97] F. Reyes-Osorio and B. K. Nikolić, Gilbert damping in metallic ferromagnets from Schwinger-Keldysh field theory: Intrinsically nonlocal, nonuniform, and made anisotropic by spin-orbit coupling, Phys. Rev. B **109**, 024413 (2024).

[98] F. Reyes-Osorio and B. K. Nikolić, Nonlocal damping of spin waves in a magnetic insulator induced by normal, heavy, or altermagnetic metallic overlayer: A Schwinger-Keldysh field theory approach, Phys. Rev. B **110**, 214432 (2024).

[99] M. Sayad and M. Potthoff, Spin dynamics and relaxation in the classical-spin Kondo-impurity model beyond the Landau-Lifschitz-Gilbert equation, New J. Phys. **17**, 113058 (2015).

[100] S. Zhang and S. S.-L. Zhang, Generalization of the Landau-Lifshitz-Gilbert equation for conducting ferromagnets, Phys. Rev. Lett. **102**, 086601 (2009).

[101] H. Y. Yuan, Z. Yuan, K. Xia, and X. R. Wang, Influence of nonlocal damping on the field-driven domain wall motion, Phys. Rev. B **94**, 064415 (2016).

[102] R. Verba, V. Tiberkevich, and A. Slavin, Damping of linear spin-wave modes in magnetic nanostructures: Local, nonlocal, and coordinate-dependent damping, Phys. Rev. B **98**, 104408 (2018).

[103] See Supplemental Material at https://wiki.physics.udel.edu/qttg/Publications for an additional Fig. S1(a) that is the counterpart of Fig. 3(b) for the case when photocurrent is allowed to excite magnons via STT, but then *sd* exchange interaction between electron spin and LMMs is quickly switched off. For easy comparison, we also analyze in Fig. S1(b) experimental data from Ref. [5] using windowed FFT.

[104] B. K. Nikolić, L. P. Zârbo, and S. Souma, Imaging mesoscopic spin Hall flow: Spatial distribution of local spin currents and spin densities in and out of multiterminal spin-orbit coupled semiconductor nanostructures, Phys. Rev. B **73**, 075303 (2006).

[105] E. Beaurepaire, G. M. Turner, S. M. Harrel, M. C. Beard, J.-Y. Bigot, and C. A. Schmuttenmaer, Coherent terahertz emission from ferromagnetic films excited by femtosecond laser pulses, Appl. Phys. Lett. **84**, 3465 (2004).

[106] T. Seifert, S. Jaiswal, U. Martens, J. Hannegan, L. Braun, P. Maldonado, F. Freimuth, A. Kronenberg, J. Henrizi, I. Radu, *et al.*, Efficient metallic spintronic emitters of ultrabroadband terahertz radiation, Nat. Photonics **10**, 483 (2016).

[107] Y. Wu, M. Elyasi, X. Qiu, M. Chen, Y. Liu, L. Ke, and H. Yang, High-performance THz emitters based on ferromagnetic/nonmagnetic heterostructures, Adv. Mater. **29**, 1603031 (2017).

[108] T. S. Seifert, D. Go, H. Hayashi, R. Rouzegar, F. Freimuth, K. Ando, Y. Mokrousov, and T. Kampfrath, Time-domain observation of ballistic orbital-angular-momentum currents with giant relaxation length in tungsten, Nat. Nanotechnol. **18**, 1132 (2023).

[109] A. Kefayati, Y. Ren, M. B. Jungfleisch, L. Gundlach, J. Q. Xiao, and B. K. Nikolić, Deciphering the origin of spin current in spintronic terahertz emitters and its imprint on their electromagnetic radiation via time-dependent density functional theory, Phys. Rev. B **111**, L140415 (2025).

[110] N. Locatelli, V. Cros, and J. Grollier, Spin-torque building blocks, Nat. Mater. **13**, 11 (2014).

[111] C. Huang, L. Luo, M. Mootz, J. Shang, P. Man, L. Su, I. E. Perakis, Y. Yao, A. Wu, and J. Wang, Extreme terahertz magnon multiplication induced by resonant magnetic pulse pairs, Nat. Commun. **15**, 3214 (2024).

[112] M. Berritta, S. Scali, F. Cerisola, and J. Anders, Accounting for quantum effects in atomistic spin dynamics, Phys. Rev. B **109**, 174441 (2024).

[113] T. Nussle, S. Nicolis, and J. Barker, Numerical simulations of a spin dynamics model based on a path integral approach, Phys. Rev. Res. **5**, 043075 (2023).

[114] E. Perfetto, Y. Pavlyukh, and G. Stefanucci, Real-time GW: Toward an *ab initio* description of the ultrafast carrier and exciton dynamics in two-dimensional materials, Phys. Rev. Lett. **128**, 016801 (2022).

[115] E. Perfetto and G. Stefanucci, Real-time GW-Ehrenfest-Fan-Migdal method for nonequilibrium 2D materials, Nano Lett. **23**, 7029 (2023).

[116] M. Bianchi, S. Acharya, F. Dirnberger, J. Klein, D. Pashov, K. Mosina, Z. Sofer, A. N. Rudenko, M. I. Katsnelson, M. van Schilfgaarde, M. Rösner, and P. Hofmann, Paramagnetic electronic structure of CrSBr: Comparison between *ab initio* GW theory and angle-resolved photoemission spectroscopy, Phys. Rev. B **107**, 235107 (2023).

[117] M. Śmiertka, M. Rygala, K. Posmyk, P. Peksa, M. Dyksik, D. Pashov, K. Mosina, Z. Sofer, M. van Schilfgaarde, F. Dirnberger, *et al.*, Unraveling the nature of excitons in the 2D magnetic semiconductor CrSBr, arXiv:2506.16426 (2025).

[118] A. Szilva, Y. Kvashnin, E. A. Stepanov, L. Nordström,

O. Eriksson, A. I. Lichtenstein, and M. I. Katsnelson, Quantitative theory of magnetic interactions in solids, Rev. Mod. Phys. **95**, 035004 (2023).
[119] F. L. Durhuus, T. Skovhus, and T. Olsen, Plane wave implementation of the magnetic force theorem for magnetic exchange constants: application to bulk Fe, Co and Ni, J. Phys.: Condens. Matter **35**, 105802 (2023).
[120] J. Li, D. Golež, G. Mazza, A. J. Millis, A. Georges, and M. Eckstein, Electromagnetic coupling in tight-binding models for strongly correlated light and matter, Phys. Rev. B **101**, 205140 (2020).
[121] G. Panati, H. Spohn, and S. Teufel, Effective dynamics for Bloch electrons: Peierls substitution and beyond, Commun. Math. Phys. **242**, 547 (2003).
[122] M. Combescot and O. Betbeder-Matibet, The effective bosonic Hamiltonian for excitons reconsidered, EPL(Europhysics Letters) **58**, 87 (2002).

## END MATTER

*Models and Methods.*—Our TDNEGF+LLG calculations are fully microscopic (i.e., Hamiltonian-based), requiring *only* two Hamiltonians as an input. These two Hamiltonians describe bare degrees of freedom—quantum Hamiltonian, $\hat{H}(t)$, for electrons; and classical one, $\mathcal{H}(t)$, for LMMs. In this study, we focus on essential features of bilayer 2D AF semiconductors [10, 11, 44] by constructing a model quantum Hamiltonian [Eq. (11)] which captures: two mononlayers, a semiconducting bandgap for each of them, ferromagnetic (FM) intralayer and AF interlayer ordering of LMMs, and possible Coulomb interaction effects [39, 40] binding conduction-band electrons and valence-band holes into excitons. Accordingly, our simulation setup in Fig. 1 consists of two one-dimensional (1D) tight-binding (TB) chains [36, 38] with two electronic orbitals per site $i$, as well as one LMM per site $i$ described by the unit vector $\mathbf{M}_i(t)$. Our usage of 1D chains is inspired by CrSBr [36–38, 78, 116] as a highly anisotropic 2D magnetic material [1, 2] formed [36, 38] by 1D atomic chains with interlayer AF ordering (A-type) and intralayer FM ordering. The Curie temperate of FM ordering within a single monolayer is $\simeq 150$ K, while AF ordering of LMMs between adjacent layers has a Néel temperature of $\simeq 130$ K [116]. Note that angle-resolved photoemission spectroscopy reveals the complex electronic band structure of CrSBr, whose accurate theoretical description can be achieved via first-principles methods [38], particularly self-consistent GW methodology [9, 116, 117].

The classical Hamiltonian, entering into the LLG Eq. (3), is given by

$$\begin{aligned}\mathcal{H}(t) \;=\; & J^{\rm AF}\sum_{\langle i\in 1, j\in 2\rangle}\mathbf{M}_i\cdot\mathbf{M}_j - J^{\rm FM}\sum_{\langle i\in 1, j\in 1\rangle}\mathbf{M}_i\cdot\mathbf{M}_j \\ & - J^{\rm FM}\sum_{\langle i\in 2, j\in 2\rangle}\mathbf{M}_i\cdot\mathbf{M}_j - K_x\sum_{i\in 1,2}(\mathbf{M}_i\cdot\mathbf{e}_x)^2 \\ & + K_z\sum_{i\in 1,2}(\mathbf{M}_i\cdot\mathbf{e}_z)^2 - J_{sd}\sum_{i\in 1,2}\mathbf{M}_i\cdot\sum_{a=c,v}\langle\hat{\mathbf{s}}_i^a\rangle \quad (10)\end{aligned}$$

Such an effective classical Heisenberg Hamiltonian of LMMs can be extracted from first-principles calculations [54, 118, 119] or by fitting magnon spectra from neutron scattering data [37]. Here $J^{\rm AF}=0.0195$ eV and $J^{\rm FM}=0.15$ eV are AF and FM exchange couplings, respectively; $K_x=0.021$ eV and $K_z=0.057$ eV specify the magnetic anisotropy along the $x$- and $z$-axis, respectively; $J_{sd}=0.01$ eV is the $sd$ exchange interaction between spin of conduction electrons and LMMs [76]; and $\langle\ldots\rangle$ denotes nearest-neighbor (NN) sites. Note that $J^{\rm AF}$, $J^{\rm FM}$, $K_x$, $K_z$ parameters were also employed to interpret experiments [3–5], but their values obtained from density functional theory calculations are rescaled by a multiplicative factor $10^3$ to make the total TDNEGF+LLG simulation time of $\sim 1$ ps duration. Nevertheless, even with this adjustment, the characteristic energy scale of the AF background remains below electron kinetic energy, $\gamma_0/J^{\rm AF}\simeq 10^2$.

The same $sd$ exchange $\hat{H}_{sd}(t)=-J_{sd}\sum_i\mathbf{M}_i(t)\cdot\sum_{a=c,v}\hat{\mathbf{s}}_{ia}$ is a term in the quantum Hamiltonian of electrons

$$\hat{H}(t)=\hat{H}_{sd}+\hat{H}_{\rm intra}+\hat{H}_{\rm inter}+\hat{H}_{\rm Coulomb}. \quad (11)$$

Here $\hat{H}_{\rm intra}$ describes 1D TB chains within layer 1 or 2 in Fig. 1

$$\begin{aligned}\hat{H}_{\rm intra} = & \Delta/2\sum_{i\in 1,2}(\hat{c}_i^{c\dagger}\hat{c}_i^c-\hat{c}_i^{v\dagger}\hat{c}_i^v) \quad (12) \\ & +\gamma_0\sum_{\langle i\in 1 j\in 2\rangle}e^{i\chi_{ij}(t)}(\hat{c}_i^{v\dagger}\hat{c}_j^v-\hat{c}_i^{c\dagger}\hat{c}_j^c)-\gamma_{\rm P}(t)\sum_{i\in 1,2}\hat{c}_i^{c\dagger}\hat{c}_i^v+{\rm H.c},\end{aligned}$$

where indices $c$ and $v$ stand for orbitals which give rise to the conduction and valence band of each chain; $\hat{c}_i^{a\dagger}=(\hat{c}_{i\uparrow}^{a\dagger}\;\;\hat{c}_{i\downarrow}^{a\dagger})$ is the row vector containing operators $\hat{c}_{i\sigma}^{a\dagger}$ which create electron with spin $\sigma=\uparrow,\downarrow$ in orbital $a=c,v$ hosted by site $i$; $\Delta$ is the onsite potential opening bandgap between the two bands $\Delta=3$ eV; and $\gamma_0=1$ eV is the hopping parameter between the NN sites. The spin density operator in Eq. (11) is given by $\hat{\mathbf{s}}_{ia}=\hat{c}_i^{a\dagger}\hat{\sigma}\hat{c}_i^a$ for $a=c,v$. The fsLP is introduced in Eq. (12) via the Peierls phase [120, 121], $\chi_{ij}(t)=z_{\rm max}\exp[-(t-t_p)^2/(2\sigma_{\rm light}^2)]\sin(\omega_0 t)$, where the electric field of the pulse is $\mathbf{E}(t)=-\partial_t\mathbf{A}(t)$, $z_{\rm max}=eaA_{\rm max}/\hbar=0.1$ is a dimensionless parameter quantifying the intensity of the pulse using $A_{\rm max}$ as the amplitude of the vector potential, $\omega_0$ is the central frequency of fsLP, and $a$ is the lattice spacing. Besides the Peierls phase, fsLP is additionally [39] introduced via hopping $\gamma_{\rm P}(t) = \mathbf{d}\cdot\mathbf{E}(t)$ in Eq. (12). This term describes those interband transitions that are driven by the dipole interaction with the electric field [39], where $\mathbf{d}$ is the expectation value of the dipole operator, $\mathbf{d} = e\langle i,c|\hat{\mathbf{r}}|i,v\rangle$. The term $\hat{H}_{\rm inter}$ is given by

$$\hat{H}_{\rm inter}(t) = -\sum_{\langle i\in 1, j\in 2\rangle}(\gamma_c \hat{c}_i^{c\dagger}\hat{c}_j^c - \gamma_v \hat{c}_i^{v\dagger}\hat{c}_j^v + \text{H.c.}), \quad (13)$$

and it describes hopping with parameter $\gamma_c = 0.5\gamma_0$ or $\gamma_v = 0.5\gamma_0$ between $c$ or $v$ orbitals, respectively, located at NN sites of two different chains. Finally, the inter-orbital Coulomb interaction [39, 40]

$$\hat{H}_{\rm Coulomb} = U \sum_{i\in 1,2;\sigma;\sigma'} \hat{n}^c_{i,\sigma}\hat{n}^v_{i,\sigma'}, \quad (14)$$

describes how two electrons on two different orbitals at the same site $i$ interact with each other. The same term was employed in prior studies [39, 40] to describe exciton formation on TB lattice. We decouple it via tMFT [40] (otherwise, its beyond-tMFT treatment requires computationally much more expensive evaluation of Feynman diagrams on the Keldysh contour [39]) as follows:

$$\begin{aligned}\hat{n}_i^c\hat{n}_i^v \;\rightarrow\; & \langle \hat{n}_i^c(t)\rangle \hat{n}_i^v + \langle \hat{n}_i^v(t)\rangle \hat{n}_i^c \\ - \; & \phi_i(t)\hat{c}_i^{c\dagger}\hat{c}_i^v - \phi_i^*(t)\hat{c}_i^{v\dagger}\hat{c}_i^c. \end{aligned} \quad (15)$$

Here the first two terms correspond to Hartree and the latter two to Fock approximation, where the order parameter of the excitonic condensate [25] is given by $\phi_i(t) = \langle \hat{c}_i^{v\dagger}(t)\hat{c}_i^c(t)\rangle$. This procedure requires to self-consistently compute $\phi_i(t)$, which we obtain from the off-diagonal elements of $\rho^{\rm neq}(t)$ as a part of TDNEGF calculations within the self-consistent loop illustrated in Fig. 2. We note that in this approach we do not rely on the effective excitonic Hamiltonians written in terms of operators of composite bosons [53], which can be cumbersome to derive [122]. Instead, we use "bare" degrees of freedom, so that both free charge carriers and excitons are considered through an electronic density matrix, as often done in other studies [39, 40, 114, 115] based on TDNEGF formalism.

The AF semiconductor CAR in Fig. 1 is attached to $L$ and $R$ NM leads modeled as semi-infinite ideal 1D TB chains with one orbital per site. The chemical potential of the macroscopic reservoirs into which NM leads terminate is identical (i.e., no bias voltage is applied) and chosen as $\mu_L = \mu_R = E_F = 0$.

The electric field of EM radiation emitted into FF region [91, 93] is calculated from the Jefimenko equations [89], reorganized [91] to isolate the contribution in FF region

$$\mathbf{E}_{\rm FF}(\mathbf{r},t) = \frac{1}{4\pi\epsilon_0 c^2}\sum_{P_{ia\rightarrow jb}=1}^{N_B}\int_{P_{ia\rightarrow jb}}\left[(\mathbf{r}-\mathbf{l})\frac{\partial_t I_{ia\rightarrow jb}(t_r)}{|\mathbf{r}-\mathbf{l}|^3}(\mathbf{r}-\mathbf{l})\cdot\mathbf{e}_x - \frac{\partial_t I_{ia\rightarrow jb}(t_r)}{|\mathbf{r}-\mathbf{l}|}\mathbf{e}_x\right]dl. \quad (16)$$

Note that Jefimenko Eq. (16) can be viewed [90] as proper (i.e., time-retarded) time-dependent generalizations of the Coulomb law. Here, $t_r \equiv t - |\mathbf{r}-\mathbf{l}|/c$ emphasizes retardation in the response time due to relativistic causality [89, 91]. Additionally, we adapt [71, 92] Eq. (16) to utilize time-dependent bond [104] charge currents as the source of EM radiation, $I_{ia\rightarrow jb}(t)$ [Eq. (17)]—they are the counterpart on TB lattice of local current density in continuous space. The bond currents $I_{ia\rightarrow jb}$ are assumed to be spatially homogeneous along the path $P_{ia\rightarrow jb}$ from orbital $a$ at site $i$ to orbital $b$ at site $j$ [65, 92, 104], which is composed of a set of points $l \in P_{ia\rightarrow jb}$. Here $N_B$ is the number of bonds $ia \rightarrow jb$, and since we use $N = 10$ black and gray sites [Fig. 2] in each layer of CrSBr, $N_B = 36$ in our calculations. We obtain bond charge currents as

$$I_{ia\rightarrow jb}(t) = \frac{e\gamma}{i\hbar}\text{Tr}_{\rm spin}\left[\rho^{\rm neq}_{ia,jb}(t)\mathbf{H}_{jb,ia}(t) - \rho^{\rm neq}_{jb,ia}(t)\mathbf{H}_{ia,jb}(t)\right]. \quad (17)$$

For this purpose, we isolate $2\times 2$ submatrices $\rho^{\rm neq}_{ia,jb}(t)$ of $\rho^{\rm neq}(t)$. Note that diagonal elements of $\rho^{\rm neq}_{ij}(t)$ determine on-site nonequilibrium charge density, whose time dependence contributes to near-field radiation [71, 92, 93].

# Supplemental Material for "Ultrafast optical excitation of magnons in 2D antiferromagnets via spin torque exerted by photocurrent of excitons: Signatures in charge pumping and THz emission"

Jalil Varela-Manjarres,[1] Yafei Ren,[1] and Branislav K. Nikolić[1,*]

[1] *Department of Physics and Astronomy, University of Delaware, Newark, DE 19716, USA*

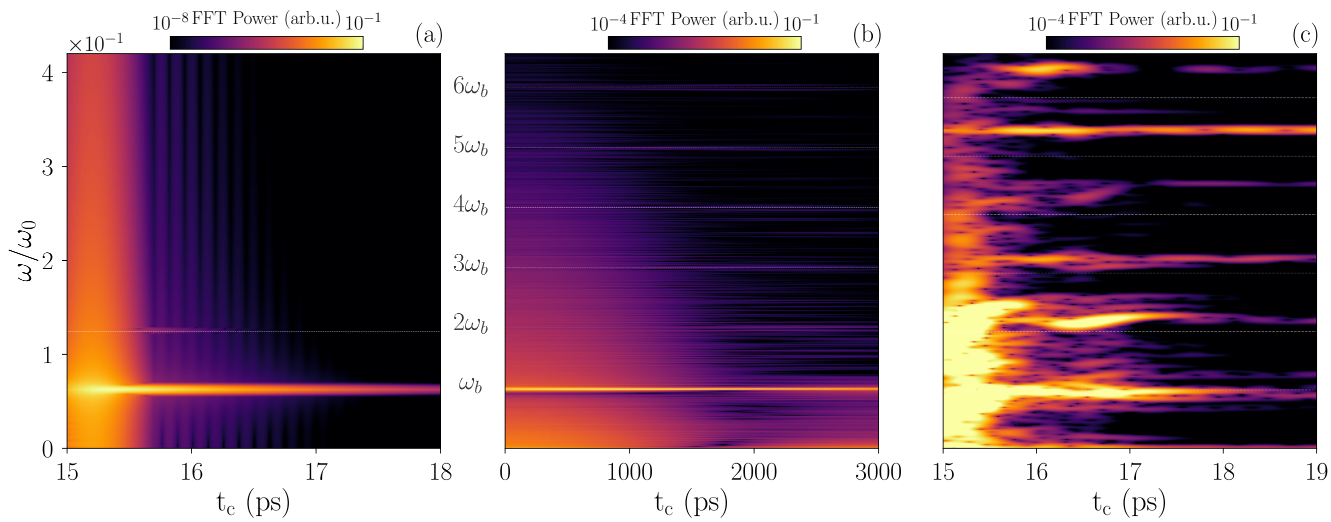


FIG. S1. Power spectrum of windowed FFT [1, 2], $|N^y(t_c,\omega)|^2$, of the $y$-component of the Néel vector [Eq. (8) in the main text] for: (a) and (c) TDNEGF+LLG-computed dynamics in the absence of excitons ($U = 0$); or (b) the same dynamics probed experimentally in CrSBr at externally applied magnetic field $B = 0.3$ T—the same data from panel (b) was analyzed in Fig. 4b of experimental Ref. [3] but using standard FFT. The dynamics of the Néel vector in panel (a) is initiated by photoexcited electrons, i.e., in the same fashion as in Fig. 3 of the main text, but then for $t \geq 15$ ps we switch off ($J_{sd} = 0$) *sd* exchange interaction between flowing electronic spins and LMMs. In panel (c), we increase the value of $J_{sd}$ used in the main text by ten times. Note that $\omega_b$ is larger in our calculations within panels (a) and (c) than in the experimental data of panel (b), so for easy comparison we rescaled the ordinate of panel (b).

This Supplemental Material provides one additional Fig. S1 consisting of three panels. Its first panel Fig. S1(a) analyzes the effect of photoexcited electrons—for simplicity, without their binding into excitons [$U = 0$ in Eqs. (11) and (14) of the main text]—on time evolution of optically excited magnons. In particular, the goal is to understand the origin of magnon peaks in Figs. 3(b) and 3(d) of the main text below the frequency $\omega_b$ of "bright magnon". For this purpose, we allow photoexcited electrons to ignite magnons microscopically (instead of adding phenomenological "impulsive perturbation" [3, 4] into the LLG equation) via spin-transfer torque (STT) exerted by electronic spin current [5–7], but then we immediately switch off interaction between flowing electronic spins and LMMs. In other words, we use the full self-consistent loop [Fig. 2 of the main text] of time-dependent nonequilibrium Green's function combined with Landau-Lifshitz-Gilbert (TDNEGF+LLG) framework before $t = 15$ ps in Fig. S1(a), and then for $t \geq 15$ ps we switch off *sd* exchange interaction so that TDNEGF and LLG parts of the loop are disconnected. Such calculations lead to a longer lifetime of magnon at frequency $\omega_b$ [3] and its second harmonic $2\omega_b$ in Fig. S1(a)—compare the length of bright lines in Fig. S1(a) at these two frequencies with their counterparts from Fig. 3(b) of the main text. The longer lifetime is the consequence of removing *nonlocal* damping [8–14], provided by the fermionic bath of electrons within TDNEGF calculations of the TDNEGF+LLG loop, when using $J_{sd} = 0$ for $t \geq 15$ ps. Otherwise, such damping is present in all figures of the main text during the whole evolution time. Note that the counterpart of $2\omega_b$ magnon visible in Fig. S1(a) is of vanishingly short lifetime in Fig. 3(b) in the main text due to nonlocal damping being operative in the latter case. The remaining finite lifetime of $2\omega_b$ magnon in Fig. S1(a) is due to retained conventional local Gilbert damping of strength $\alpha_G$ [Eq. (3) of the main text]. Importantly, switching off *sd*

* bnikolic@udel.edu

interaction between flowing electronic spins and LMMs also *removes* [Fig. S1(a)] bright lines of excited magnons that are otherwise present in Fig. 3(b) of the main text at frequencies below $\omega_b$. This finding confirms that magnons peaks below $\omega_b$ are due [15] to photoexcited electrons, which are explicitly included in our TDNEGF+LLG framework, but are absent from the LLG equation used on its own in Fig. S1(a) for $t \geq 15$ ps.

For comparison, we apply windowed FFT [1, 2] to experimental data from Ref. [3] generated in the course of detection of optically excited magnons in CrSBr. Such analysis replicates in Fig. S1(b) "bright magnon" at frequency $\omega_b$, while additionally (in comparison with standard FFT performed in Ref. [3]) revealing its long lifetime. We also unravel shorter-living magnons at high harmonics $n\omega_b$. However, the power spectrum of windowed FFT is too noisy in Fig. S1(b) for frequencies below $\omega_b$ to allow us to extract additional magnon peaks expected [Figs. 3(b) and 3(d) of the main text] to be excited due to flowing electronic spins interacting with LMMs. We speculate that magnon peaks below $\omega_b$ frequency could be present in experiments, but they are short-lived and, therefore, invisible to the standard FFT employed in Ref. [3].

Finally, in contrast to Fig. S1(a) where $J_{sd}$ is abruptly reduced to zero for $t \geq 15$ ps, in Fig. S1(c) we keep it nonzero for all times while increasing it ten times ( $J_{sd} = 0.1$ eV) when compared to the same *sd* exchange interaction between flowing electronic spins and LMMs used in the main text (where $J_{sd} = 0.01$ eV). This choice leads to high harmonic generation (HHG) in Fig. S1(c), but at frequencies that are not exact integer multiples $n\omega_b$. While this finding does not match integer harmonics observed experimentally [3] and reproduced in Fig. S1(b), it does offer hints for future extensions of TDNEGF+LLG framework and its application to HHG of magnons, as discussed in the main text.


[1] W. H. Press, S. A. Teukolsky, W. T. Vetterling, and B. P. Flannery, *Numerical Recipes: The Art of Scientific Computing* (Cambridge University Press, Cambridge, 2007).

[2] M. X. Cohen, *Analyzing Neural Time Series Data: Theory and Practice* (The MIT Press, Cambridge,, 2014).

[3] G. M. Diederich, M. Nguyen, J. Cenker, J. Fonseca, S. Pumulo, Y. J. Bae, D. G. Chica, X. Roy, X. Zhu, D. Xiao, Y. Ren, and X. Xu, Exciton dressing by extreme nonlinear magnons in a layered semiconductor, Nat. Nanotechnol. **20**, 617 (2025).

[4] X.-X. Zhang, L. Li, D. Weber, J. Goldberger, K. F. Mak, and J. Shan, Gate-tunable spin waves in antiferromagnetic atomic bilayers, Nat. Mater. **19**, 838 (2020).

[5] D. Ralph and M. Stiles, Spin transfer torques, J. Magn. Magn. Mater. **320**, 1190 (2008).

[6] B. K. Nikolić, K. Dolui, M. Petrović, P. Plecháč, T. Markussen, and K. Stokbro, First-principles quantum transport modeling of spin-transfer and spin-orbit torques in magnetic multilayers, in *Handbook of Materials Modeling*, edited by W. Andreoni (Springer, Cham, 2018) pp. 1–35, arXiv:1801.05793.

[7] K. D. Belashchenko, A. A. Kovalev, and M. van Schilfgaarde, First-principles calculation of spin-orbit torque in a Co/Pt bilayer, Phys. Rev. Mater. **3**, 011401 (2019).

[8] U. Bajpai and B. K. Nikolić, Time-retarded damping and magnetic inertia in the Landau-Lifshitz-Gilbert equation self-consistently coupled to electronic time-dependent nonequilibrium green functions, Phys. Rev. B **99**, 134409 (2019).

[9] F. Reyes-Osorio and B. K. Nikolić, Gilbert damping in metallic ferromagnets from Schwinger-Keldysh field theory: Intrinsically nonlocal, nonuniform, and made anisotropic by spin-orbit coupling, Phys. Rev. B **109**, 024413 (2024).

[10] F. Reyes-Osorio and B. K. Nikolić, Nonlocal damping of spin waves in a magnetic insulator induced by normal, heavy, or altermagnetic metallic overlayer: A Schwinger-Keldysh field theory approach, Phys. Rev. B **110**, 214432 (2024).

[11] M. Sayad and M. Potthoff, Spin dynamics and relaxation in the classical-spin Kondo-impurity model beyond the Landau-Lifschitz-Gilbert equation, New J. Phys. **17**, 113058 (2015).

[12] S. Zhang and S. S.-L. Zhang, Generalization of the Landau-Lifshitz-Gilbert equation for conducting ferromagnets, Phys. Rev. Lett. **102**, 086601 (2009).

[13] H. Y. Yuan, Z. Yuan, K. Xia, and X. R. Wang, Influence of nonlocal damping on the field-driven domain wall motion, Phys. Rev. B **94**, 064415 (2016).

[14] R. Verba, V. Tiberkevich, and A. Slavin, Damping of linear spin-wave modes in magnetic nanostructures: Local, nonlocal, and coordinate-dependent damping, Phys. Rev. B **98**, 104408 (2018).

[15] F. Reyes-Osorio and B. K. Nikolić, Bringing light into the Landau-Lifshitz-Gilbert equation: Consequences of its fractal non-Markovian memory kernel for optically induced magnetic inertia and magnons, arXiv:2504.17769 (2025).